Title
The ultrafast X-ray spectroscopic revolution in chemical dynamics

Journal
Nature Reviews Chemistry, 2(6)

ISSN
2397-3358

Authors
Kraus, PM
Zürch, M
Cushing, SK
et al.

Publication Date
2018-06-01

DOI
10.1038/s41570-018-0008-8

Peer reviewed

The Ultrafast X-ray Spectroscopic Revolution in Chemical Dynamics

Peter M. Kraus,[1,*] Michael Zürch,[1] Scott K. Cushing,[1,2]
Daniel M. Neumark,[1,2,†] and Stephen R. Leone[1,2,3,‡]

[1]*Department of Chemistry, University of California, Berkeley, CA 94720, USA*
[2]*Chemical Sciences Division, Lawrence Berkeley National Laboratory, Berkeley, CA 94720, USA*
[3]*Department of Physics, University of California, Berkeley, CA 94720, USA*

(Dated: February 21, 2018)

Abstract

The last two decades have seen rapid developments in short-pulse x-ray sources, which have enabled the study of chemical dynamics by x-ray spectroscopies with unprecedented sensitivity to nuclear and electronic degrees of freedom on all relevant time scales. In this perspective, some of the major achievements in the study of chemical dynamics with x-ray pulses produced by high-harmonic, free-electron-laser and synchrotron sources on time scales from attoseconds to nanoseconds are reviewed. Major advantages of x-ray spectral probing of chemical dynamics are unprecedented time resolution, element and oxidation state specificity and - depending on the type of x-ray spectroscopy - sensitivity to both the electronic and nuclear structure of the investigated chemical system. Particular dynamic processes probed by x-ray radiation, which are highlighted in this perspective, are the measurement of electronic coherences on attosecond to femtosecond time scales, time-resolved spectroscopy of chemical reactions such as dissociations and pericyclic ring-openings, spin-crossover dynamics, ligand-exchange dynamics, and structural deformations in excited states. X-ray spectroscopic probing of chemical dynamics holds great promise for the future due to the ongoing developments of new types of x-ray spectroscopies such as four-wave mixing and the continuous improvements of the emerging laboratory-based high-harmonic sources, and large-scale facility-based free-electron lasers.

*peter.kraus@berkeley.edu
†dneumark@berkeley.edu
‡srl@berkeley.edu

I. THE X-RAY SPECTROSCOPIC REVOLUTION

Time-resolved experimental techniques have played a major role in our fundamental understanding of chemical processes. Temperature jump [1] and flash photolysis methods [2] were rigorously explored in the 1950's. Their application led to the successful investigation of reactive free radicals and other transient species, as well as the study of fast ionic reactions such as the association of protons and hydroxide to form water. The success of those methods, employing only incoherent light sources at the time, culminated in the Nobel Prize in Chemistry in 1967 for Manfred Eigen, Ronald George Wreyford Norrish and George Porter "for their studies of extremely fast chemical reactions, effected by disturbing the equilibrium by means of very short pulses of energy" [3]. These studies were mainly concerned with species and reactions occurring on the microsecond to nanosecond time scale.

Ultrafast lasers can reveal even faster processes and provide access to the fundamental time scales of the making and breaking of a chemical bond. Pump-probe experiments were developed to record the real-time evolution of photochemical reactions in order to follow nuclear dynamics on electronically excited potential energy surfaces [4–7] and to spectrally characterize transient species [8] during such reactions. These breakthroughs led to another Nobel Prize in Chemistry, which was awarded in 1999 to Ahmed H. Zewail "for his studies of the transition states of chemical reactions using femtosecond spectroscopy" [9].

After these tremendously successful eras of studying chemical dynamics, one can ask where the next frontier areas lie. Considerable efforts are underway to develop techniques to "make a molecular movie", in which one images the evolving geometric structure of a molecule undergoing a reaction. X-ray diffraction and scattering [10] as well as electron diffraction methods [11] have been developed to study transient nuclear structures during electrocyclic reactions [10] and photoinduced elimination reactions [11], and to image the atomic scale motion during a molecular dissociation [12]. While these methods can provide superb information on evolving nuclear geometries, another important aspect of chemical reactivity is the evolving electronic structure, the dynamics of which can occur on time scales as fast as attoseconds. Electron dynamics can be probed by powerful spectroscopic methods. Possibly the ultimate goal of studying photochemical reaction dynamics would be to instantly remove or excite an electron in a complex molecule, and subsequently follow how the initial photoexcitation first launches electron dynamics, and finally resolves into

nuclear dynamics and bond-breaking. In this perspective, it is outlined how emerging x-ray spectroscopic techniques can be applied to accomplish this challenge and to follow both the electronic and nuclear structure of chemical complexes undergoing dynamical processes.

Generally, the probing wavelength in an ultrafast experiment determines which transitions are probed between initial and final states during a chemical process, and thus what aspects of a reaction are monitored. Many spectroscopic techniques with visible and infrared light have been developed that probe transitions between valence states and vibrational levels, respectively. X-ray spectroscopy on the other hand can elucidate dynamics by probing transitions from an inner shell core orbital into a valence state. These localized core-level transitions are element-specific and thus rely on reporter atoms to follow dynamical processes [13]. The core level can be subject to energy shifts during chemical reactions, when the oxidation state of the atom and thus the effective screening of the core-hole potential changes; this makes x-ray spectroscopy a sensitive tool to follow charge state dynamics, oxidation states and spin states of atoms and molecules. In favorable cases, the steep change in energy with internuclear separation of core level potentials can even provide information about bond length changes directly via shifts in core-level transition energies [14–16]. If the screening of the core-hole potential does not change much during a dynamical process, energy shifts of the core-level are negligible compared to valence-shell dynamics, which can make core-level spectroscopies a selective tool for following valence shell processes.

Besides the noted advantageous properties of x-rays for probing chemical dynamics, another major driving force at work in the x-ray spectral region is the possibility to generate shorter pulses than in the visible spectral range [17]. Attosecond pulses [18], which are at the current frontier of ultrashort pulse generation, can measure purely electronic dynamics before the onset of any nuclear motion. High-harmonic generation (HHG) based x-ray sources can enable ultrashort pulses of a few tens of attoseconds duration [19–23], with the shortest currently reported pulse duration being 43 as [23]. In the past autocorrelation measurements of x-ray free electron lasers (FELS) by two-photon ionization have demonstrated pulse durations on the order of 30 fs [24, 25], and photoelectron streaking measurements revealed that some x-ray pulses were on average no longer than 4.4fs [26]. The latest developments are pushing these pulse durations down to the sub-fs range, and single-spike hard x-ray pulses with a bandwidth supporting pulse durations of about 200 as have been generated [27]. Synchrotron based experiments can employ femtosecond slicing techniques to obtain pulse

durations in the range of tens to hundreds of femtoseconds [28]. While FEL and synchrotron experiments [29, 30] are carried out at large-scale facilities, HHG based experiments have the additional advantage that they can be realized in a table-top laboratory setting.

In this perspective, the relevant time scales and processes of photoinduced chemical dynamics will be discussed. Examples of processes on all relevant time scales, from attoseconds to nanoseconds, will be presented and the relevant x-ray techniques to probe these processes will be illustrated (Fig. 1). This perspective highlights what x-ray spectroscopic methods can contribute in resolving chemical dynamics, while not being a complete review of all available studies of chemical dynamics with x-rays. The perspective primarily focuses on molecular species, rather than materials, for which x-rays also offer similarly exquisite new determinations of time dynamics [31–40].

II. X-RAY TECHNIQUES FOR FOLLOWING CHEMICAL DYNAMICS

Figure 1 illustrates the relevant time scales of photo-induced chemical dynamics. The fastest processes relevant to chemical dynamics are lifetimes of highly excited states and delays in photoemission [41–43]. Attosecond photoelectron interferometry techniques are powerful in measuring such delays. These techniques are based on extreme ultraviolet (XUV)/x-ray photoionization, and using a phase-locked near-infrared pulse to modulate the momentum of the outgoing electron to exactly time its moment of release.

If the lifetimes of the excited states are long enough [44], the preparation of a manifold of electronically excited states can launch coherent electron dynamics. X-ray emission techniques such as high-harmonic spectroscopy (HHS) rely on the precisely timed sub-cycle ionization, acceleration and recombination [45, 46] of one of the valence electrons in the investigated atom or molecule. While the process of ionization can induce dynamics, the photorecombination process can be interpreted as time-reversed photoionization, which is thus very sensitive to the electronic structure of the evolving transient species. This allows the process of HHG to be employed as a unified pump-probe scheme. This idea was first used to follow the nuclear motion of the hydrogen atoms in H_2 following strong-field ionization with a resolution of about 100 as by comparing the HHG spectra of H_2 and D_2 [46]. This technique has been further developed to follow the periodic relaxation of an electron hole in CO_2 [47] and N_2 [48], as well as charge migration in the molecule HCCI [49]. Independently,

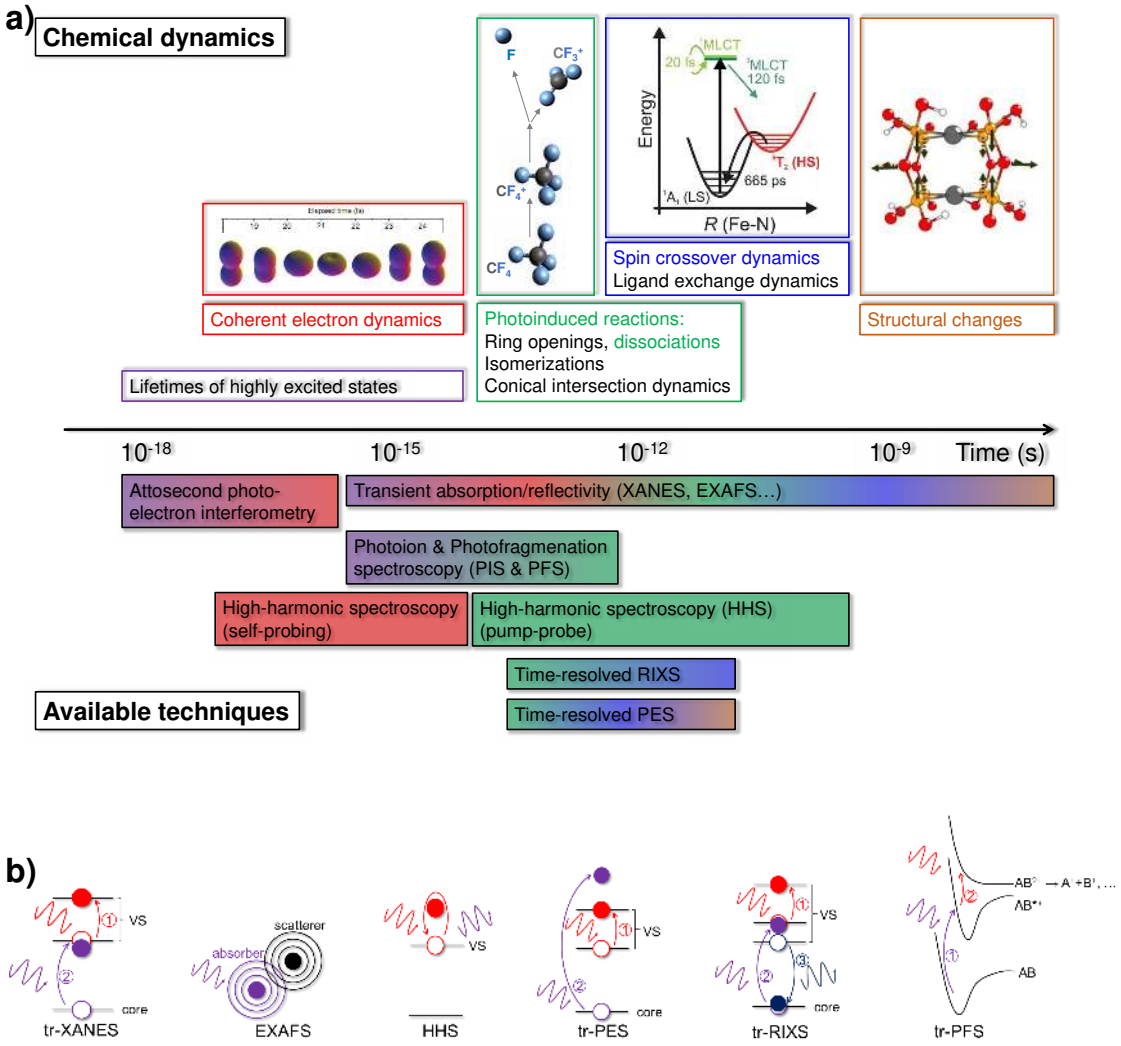

FIG. 1: **X-ray spectroscopy of chemical dynamics:** (a) Chemical dynamic processes occur on different time scales spanning from attoseconds (10^{-18} s) to nanoseconds (10^{-9} s). Various x-ray techniques are suited to investigate the different processes on all time scales. (b) Illustration of the different x-ray techniques that can be used in time-resolved (tr) experiments to measure chemical dynamics.

HHS has been demonstrated to be very sensitive to the electronic structure of atoms and molecules through the photorecombination dipole moment, which was used for tomographic imaging of molecular orbitals [50, 51], and to measure photorecombination resonances [52–54] and laser-modified electronic structures [55]. Moreover, generating high harmonics with an infrared pulse from a photoexcited sample can be employed as a probe in a pump-probe

experiment. The sensitivity of HHG to the evolving electronic structure of photoexcited molecules enables photochemical studies of dissociations [56, 57] and conical intersections [58–60]. Recent advances in solid-state high-harmonic generation [61] have pointed out opportunities to extend this technique for measurements of transient band structure changes [62] and phase transitions in strongly correlated materials [63].

Electronic dynamics and coherences can also be studied by time-resolved x-ray absorption near-edge structure (tr-XANES) spectroscopy. XANES measures the electronic structure from the viewpoint of a reporter atom in terms of the joint density of states (jDOS) between a core level and an empty valence state. Importantly, the frequency resolution of XANES is not limited by the bandwidth of the laser pulses, but rather is given by the natural linewidth of the transitions, because the measurement of an absorption line can be interpreted as the interference between the x-ray radiation and the induced x-ray polarization [64]. Thus XANES is very popular for investigations on all timescales. Examples in this perspective include the measurement of coherent electron dynamics [65] on the attosecond to femtosecond time scale, photodissociation and electrocyclic ring-opening dynamics on the tens to hundreds of fs time scale [66, 67], and spin-crossover dynamics on the femtosecond to picosecond time scale [68].

While XANES provides information on the electronic structure from the viewpoint of a reporter atom, extensions of this technique to several tens to a hundred eV above the onset of an absorption edge can specifically reveal information on the nuclear structure. This extended x-ray absorption fine structure (EXAFS) is sensitive to the scattering of a photoelectron with neighboring atoms, and the intensity modulations report on the geometry in the vicinity of the reporter atom [69]. Such structural changes typically occur on slower time scales, and an example considered in this perspective describes structural changes in photoactivated diplatinum complexes on picosecond to nanosecond time scales. As noted, nuclear dynamics are also obtained via XANES through the dependence of the core level transition energy on internuclear separation [14–16]. Thus optical x-ray absorption spectroscopy in the form of XANES or EXAFS can already provide information on all relevant time-scales down to attoseconds, with sensitivity to electronic and nuclear dynamics.

Instead of analyzing the absorbed light, x-rays emitted from the sample can be detected. In x-ray emission spectroscopy (XES) [70], an x-ray photon is used to create a core-hole, and subsequently x-ray fluorescence or resonant inelastic x-ray scattering processes (RIXS) are

detected. An example for RIXS is given below. X-ray emission occurs due to the transition from valence orbitals to the core hole, and thus reflects the density of occupied states, whereas x-ray absorption measures unoccupied states as described in the last paragraphs. This sensitivity to occupied states was used to track the photosynthetic O_2 formation in the photosystem II on μs timescales and to identify the previously postulated but unobserved S_4 state in the oxygen evolution cycle [71].

Other techniques besides absorption can be very beneficial in elucidating chemical dynamics. Photoemission techniques allow to directly ionize core electrons instead of observing core-to-valence transitions, and the method has the additional benefit of exclusively tracing the dynamics of charge state changes and interfacial charge transfer [72, 73]. Photoemission techniques in the XUV and x-ray are capable of measuring femtosecond to nanosecond dynamics [74–76]. Apart from core-level photoelectron studies, x-rays can be tremendously useful for valence-state photoemission. The high photon energies allow to map a large inverse space of the band structure of investigated materials in angle-resolved photoemission spectroscopy (ARPES) studies [77]. Time-resolved ARPES with XUV pulses [78, 79] generated by HHG for valence shell photoemission have been successfully applied to measure light-induced phase transitions [80] and to identify mechanisms for light-induced phase transitions [81], and new high-repetition rate narrowband HHG sources [82] pave the way towards studies of electron dynamics in novel materials.

Charge transfer following photoexcitation or photoionization can occur on few-femtosecond time scales and can be monitored with high temporal resolution through photofragmentation studies [83, 84]. This technique was applied to measure dynamics in the phenylalanine cation, where XUV pulses first ionized phenylalanine, and subsequent IR pulses probe the dynamics by ionizing the system to a state of the dication, which subsequently dissociates [84, 85]. The modulations in one of the fragment ions versus time delay reveal the evolution of the charge density following ionization.

Complicated spin crossover dynamics can be resolved by XANES [68], but in complex systems passage through multiple chemically similar transition states cannot always be resolved by simple absorption measurements. Resonant inelastic x-ray scattering (RIXS) is a new powerful x-ray emission technique that can solve this problem. In RIXS x-ray pulses are used to core-excite the sample, the core-hole is subsequently refilled by a valence electron, and the spectrum of the subsequent x-ray emission is detected as a function of the incident x-ray

photon energy. This can be understood as an x-ray scattering technique, which leaves the sample in an excited state and effectively probes the valence shell transitions by measuring the energy difference of incoming and outgoing photons, thus minimizing the effect of core hole shifts. First time-resolved studies using RIXS were applied to resolve ligand-exchange and spin-crossover dynamics in a solution of $Fe(CO)_5$ in ethanol (EtOH) [86], discussed in detail in this perspective.

An in-depth discussion of some of the examples mentioned in this section is provided in the following sections.

TABLE I: Overview of available short-pulse x-ray light sources.

	Photon energy	**Pulse energy**	**Repetition rate**	**Average Power**	**Pulse duration**
HHG	<1.5 keV [87], significant flux for time-resolved experiments at <450 eV [66, 67, 88]	10 μJ (at 10 Hz, 20 eV) [89, 90], typically <1 nJ at 1 kHz [90–92]	Up to 80 MHz [93]	<10 μW [93, 94], 1 mW expected [95]	43 as (at 100 eV) [23]
FEL	<24 keV (0.5 Å) [96, 97]	Up to 1 mJ	≈100 Hz, 27 kHz and 1 MHz planned [96]	up to 120 mW [96, 97]	4.4 fs [26], Bandwidth supports 200 as [27]
Synchrotron (time sliced)	<100 keV [98]	1 nJ [98]	1-10 kHz [98]	10 μW [98]	100 fs [98]

Before concluding this section, a brief discussion on the technical constraints of different x-ray sources is provided here. As mentioned earlier, only HHG sources can be realized in a table-top setting, and those currently provide the best time resolution [21, 23]. Further characteristic and current state-of-the-art parameters of HHG, FEL and synchrotron sources are summarized in Table I. While HHG sources are hugely advantageous due to their compactness and short pulse durations, their main drawback is the inefficiency of the HHG process and the low pulse energies. However, comparatively high average powers on the order of <1mW for MHz repetition rates can currently be generated by XUV frequency combs, which rely on coupling an IR frequency comb into an XUV enhancement cavity [99, 100]. New high-energy and high-power x-ray sources are currently developed in the ELI-ALPS facility, which will be run as a user facility and be the first facility of its kind for HHG experiments [101, 102]. Free electron lasers can provide much higher pulse energies up to mJ levels, but these are currently limited to rather low repetition rates (≈100 Hz). The new LCLS II and European XFEL FELs will be the first high repetition rate FELs at 1 MHz and 27 kHz, respectively [97]. A good summary of the parameters for all FELs operating in the x-ray regime is given on the XFEL homepage [96]. The biggest advantage

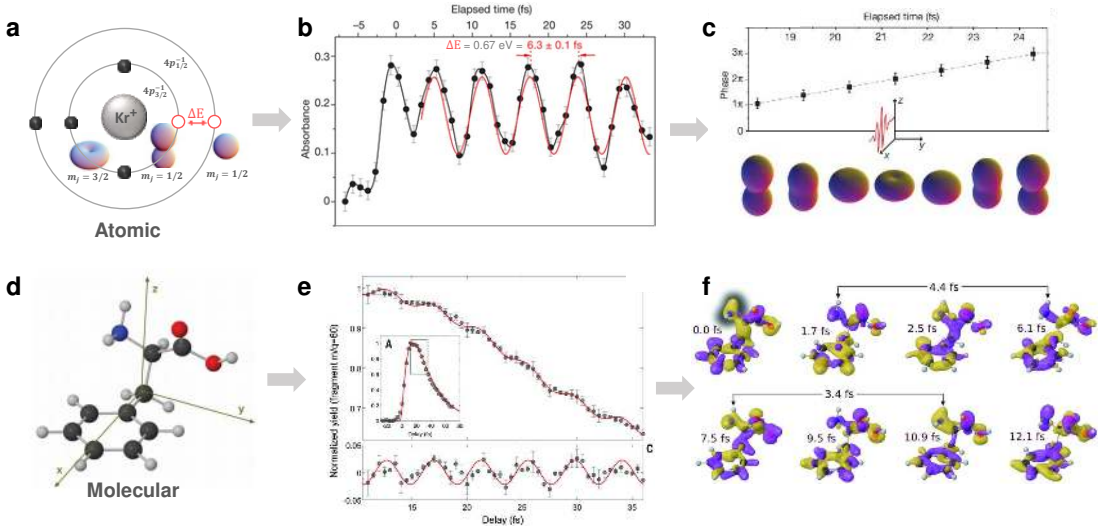

FIG. 2: **Electronic coherences measured in atoms and molecules:** (a) Schematic of the 4p shell holes in the krypton ion as excited by the visible light laser pulse. The XUV probe, not shown, measures transitions to the 3d shell. The energy splitting between the $4p_{3/2}^{-1}$ and $4p_{1/2}^{-1}$ is shown. (b) This energy splitting leads to the coherent oscillations as measured by the $4p_{3/2}^{-1} \leftarrow 3d_{3/2}^{-1}$ transition. (c) The quantum phase and ensemble-averaged hole density distributions in the $4p$ sub-shell as reconstructed from the measured coherence and a density matrix model. (d) Molecular structure of the aromatic acid phenylalanine with carbon shown as dark gray spheres; hydrogen as light grey; nitrogen as blue; oxygen as red. (e) Yield of doubly charged immonium ions following excitation with an attosecond pump, with the inset showing an exponential rise and decay fit, and the bottom panel showing the extracted coherence of 4.3 fs period. (f) Time-averaged hole density following attosecond ionization. The amine group measured in (e) is shaded in the first panel, and the origin of the measured electronic-wavepacket coherence is indicated. Panels (a) - (c) are adapted from ref. [65], and panels (d) - (f) are adapted from ref. [84].

of current femtosecond synchrotron sources is their availability, their wavelength tunability, and the high repetition rates, which are favorable for time-resolved experiments. However, the femtosecond-slicing technique [28] inherently limits the available pulse energies.

III. ATTOSECOND TRACKING OF COHERENT ELECTRON MOTION

Electronic coherences can be thought to be a primary quantum response of a system following short-pulse light-matter interaction. After photoexcitation, the quantum states are initially coherent, which leads to an oscillatory evolution of the electron density and related spectroscopic observables. Macroscopic kinetics, described by exponential decay processes, can subsequently set in, when the coherences have dephased or the energy has coupled to other available degrees of freedom. Vibronic couplings, i.e. the coupling of electronically excited states in a molecule through nuclear degrees of freedom, can cause dephasing of an electronic coherence on timescales as fast as one femtosecond [103]. Nevertheless, long-lived coherences exist, and this exciting observation has been speculated to play a significant role in light-induced photosynthetic energy transfer [104], which is still a hot and debated topic today [105]. Besides the application of photosynthetic energy transfer, the possibility to observe decoherence rates in coherently excited systems has tremendous applications in quantum information and quantum computing. Applications in these fields typically aim at creating a binary entangled state, and preserving the excited coherence for a given time [106–108].

Attosecond spectroscopy is capable of directly tracking the coherent quantum evolution of systems (Fig. 2). In 2010 a first pioneering experiment investigated the quantum evolution of an electron hole in ionized krypton atoms. In this experiment a sub-5 fs near-infrared pump pulse was used to strong-field ionize krypton, preparing the cation in the spin-orbit split states with an electron hole in the $4p^{-1}_{(3/2)}$ and $4p^{-1}_{(1/2)}$ states, which are split by an energy separation of $\Delta E = 0.67$ eV corresponding to an oscillation period of the hole density of $\tau = h/\Delta E = 6.3$ fs. This periodic oscillation was probed by XUV core-to-valence band transitions. The XUV attosecond pulses promoted $3d$ core electrons into the $4p^{-1}_{(3/2)}$ and $4p^{-1}_{(1/2)}$ vacancies, which resulted in a periodic modulation of the XUV absorbance as a function of the pump-probe delay due to the periodically changing alignment of the p-hole superposition state. The combined observation of the amplitude and phase of the oscillations allowed to reconstruct the evolution of the electron-hole density as a function of the pump-probe delay.

Coherent attosecond electron dynamics in more complex systems have gained considerable interest in recent years. Attosecond charge migration, which describes a purely elec-

tronic oscillating coherent motion following ionization, as opposed to charge transfer, which also involves nuclear motion, was investigated theoretically [109–111]. In particular, theoretical analyses showed that attosecond charge migration can be linked to strong electron correlations in molecules [110, 112–115]. Ultrafast electron dynamics following ionization were investigated experimentally by attosecond spectroscopy through photoionization and fragmentation techniques. The amino acid phenylalanine was ionized by an XUV attosecond pulse, and a subsequent near-infrared pulse was used to produce the dication through multiphoton ionization. This experiment revealed an oscillation in the yield of the immonium dication versus time delay, which is one of the fragmentation products resulting from the dissociation of the dication. Comparison to time-dependent density functional theory (TDDFT) simulations related this oscillation to a complex electronic motion.

While the results in krypton illustrate that the coherent electronic wave packet lives for a long time and will only dephase once the atoms collide in the gas phase, the coherent electron oscillations in phenylalanine clearly dephase much more rapidly in about 40 fs. The reason for this is the redistribution of the electronic excitation into other states by passage through conical intersections mediated by vibronic couplings, and generally the dephasing of electronic coherences through nuclear motion. This redistribution of the electronic excitation energy can then further induce reactions and more complex chemical dynamics, which are discussed in the next sections.

IV. FEMTOSECOND PHOTOCHEMICALLY INDUCED PROCESSES

Femtosecond XANES is ideally suited to follow photochemical dynamics. The changes in the electronic environment of a reporter atom during a chemical reaction lead to energy shifts of the absorption edges, which can be employed to track the photochemical processes. Recently, pioneering HHG-based experiments studied the femtosecond dynamics of electrocyclic ring-openings and dissociations at the x-ray carbon K-edge [66, 67]. These examples are shown in Fig. 3.

Cyclohexadiene is photoexcited by 266 nm (Fig. 3a), 100 fs laser pulses from its 1A ground state to the 1B excited state by promoting an electron from the 2π HOMO to the $1\pi^*$ LUMO (Fig. 3b). Subsequently the system relaxes through two conical intersections with an intermediate 2A transition state, where the $1\pi^*$ orbital is doubly occupied and

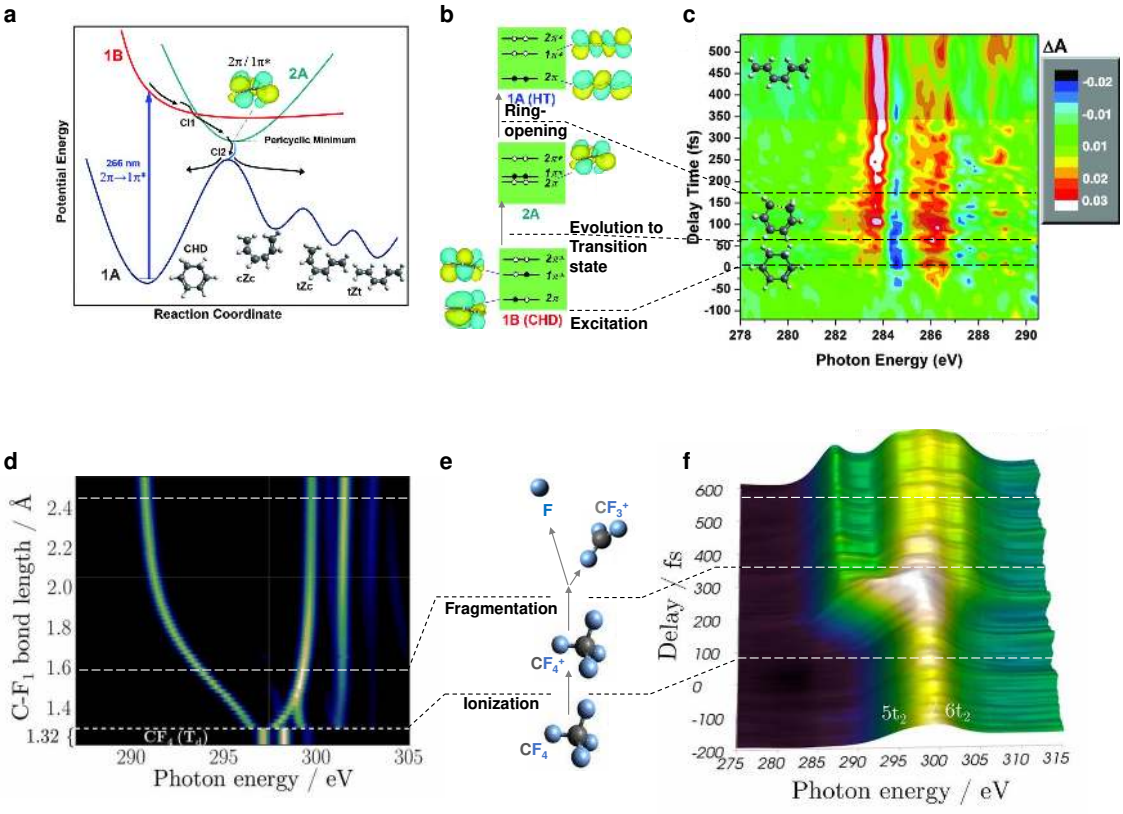

FIG. 3: **Following a chemical reaction with soft x-ray spectroscopy:** (a) Schematic view of the potential energy surfaces of ground state and photoexcited cyclohexadiene (CHD), which undergoes an electrocyclic ring-opening through conical intersections. The relevant electronic configurations of the transition states of the photochemical reaction are shown in (b). (c) Experimental transient absorption spectrum of CHD in the water window at the carbon-K edge. (d) Calculated x-ray absorption versus bond length of the light induced $CF_4^+ + \rightarrow CF_3^+ + F$ reaction, which is shown schematically in (e). (f) Experimental transient absorption spectrum in the water window at the carbon k edge. The experimental trace in time mirrors the theoretical prediction based on bond length. Adapted from refs. [66] and [67].

the 2π unoccupied, back to the 1A ground-state of hexatriene, which has an open ring. This evolution is tracked through the transient XANES signal (Fig. 3c), which reveals the preparation of the 2A state (the so-called pericyclic minimum, see Fig. 3a) to proceed within 60±20 fs and to subsequently decay within 110±60 fs to the 1A ground state of cyclohexatriene. In a similar way, the femtosecond intersystem crossing in acetylacetone could be tracked via x-ray transient absorption at the carbon K-edge [116].

In an example shown in Fig.3d-f, a strong NIR pulse ionizes CF_4 molecules, which subsequently dissociate into CF_3^+ cations and F atoms (Fig. 3e). The dissociation breaks the symmetry of the system and thus leads to the appearance of a new x-ray spectral line in carbon (Fig. 3f) at lower energies, and the carbon K-edge x-ray transition probes the evolution from a tetrahedral carbon atom to one with a trigonal planar chemical environment. The transient absorption spectrum (Fig. 3f) mimics the changes in the distance of the dissociating C-F bond (Fig. 3d) and the simultaneous relaxation of the coordinates of the other three fluorine atoms.

The generality of femtosecond XANES was furthermore demonstrated by many other studies that have measured the evolution of vibrational wave packets in molecular bromine following strong-field ionization [14], the strong-field-ionization induced ring opening of selenophene [117], the ionization-induced dissociation of dibromomethane and ferrocene [118, 119], and the evolution of transition states during the dissociation of methyl iodide [120]. These measurements were done at element specific absorption edges in the XUV between 40-70 eV.

The current limitations of high-harmonic sources are mainly rooted in the low photon flux at high photon energies. While HHG radiation up to >1 keV has been demonstrated [87], x-ray pump-probe studies around 300 eV at the carbon K edge have recently been established [66, 67, 116], and the achievable limits are being pushed continuously to higher and higher energies currently approaching the titanium L-edge around 450 eV [88]. Synchrotrons and FELs are sources that can provide much higher photon energies. While synchrotrons are intrinsically narrow band sources, the development of femtosecond slicing in 2001 [28] enabled synchrotron based studies with sub 100 fs time resolution. First femtosecond x-ray absorption studies subsequently addressed the photoinduced phase transition in VO_2 [121], which could be simultaneously followed at the Vanadium L-edge and oxygen K-edge.

The new capabilities of femtosecond slicing techniques were applied to study spin-crossover dynamics. Spin crossover is a ubiquitous and heavily researched phenomenon in Fe(II) complexes, which can generally occur following photoexcitation. Within a ligand-field theory description of the iron complex, the metal d orbitals are arranged as triply degenerate t_{2g} and doubly degenerate e_g orbitals, which are occupied by six valence electrons of the Fe(II) complex, and five valence electrons for a photochemically reduced Fe(III) complex (lower panel in Fig. 4a). If the magnitude of the ligand field splitting (energy difference

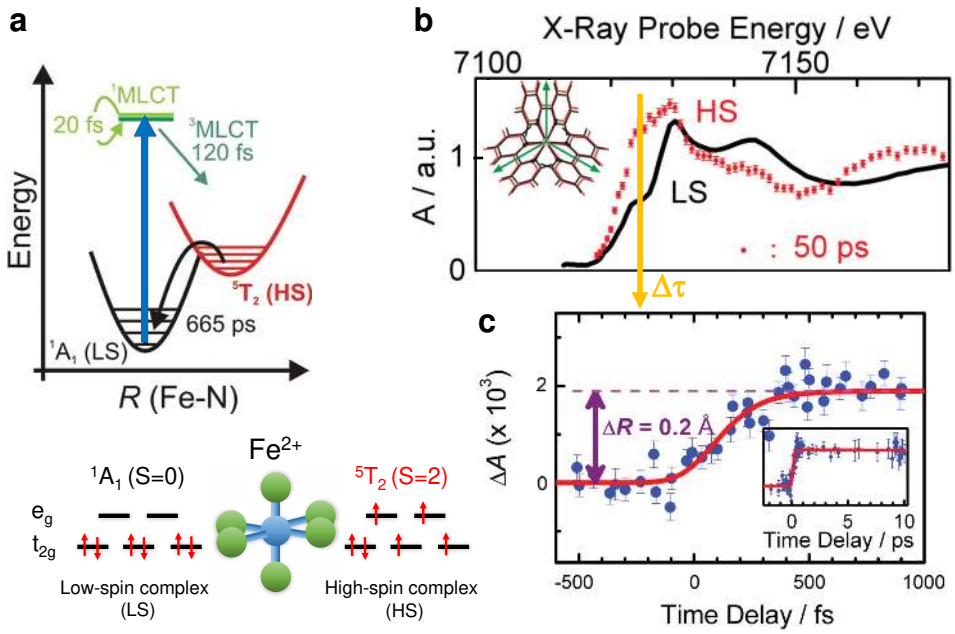

FIG. 4: **Time-resolved XANES measurement of spin crossover dynamics in aqueous Iron(II)-tris(bipyridine) ($[Fe(II)(bpy)_3]^{2+}$):** (a) Schematic of the potential energy surfaces along the Fe-N bond distance and relaxation cascade following photo-excitation by a 400-nm laser pulse (blue arrow). The initial excitation from the low spin (LS) state $^1A_1$ into the singlet metal-to-ligand-charge-transfer (^{1}MLCT) is followed by an intersystem crossing into the triplet ^{3}MLCT and subsequent relaxation into the lowest excited quintet or high spin (HS) state $5T_2$ with the time scales indicated. (b) The spin crossover can be directly studied at the Fe K-edge, where the resulting bond lengthening (indicated in inset) causes changes in the XANES spectrum with most significant changes near the absorption edge (orange arrow). (c) Ultrafast time-resolved measurement by varying the time delay (Δt) at a fixed photon energy employing femtosecond time slicing at a synchrotron allows measuring the time scale of the spin crossover to approximately 250-300 fs and comparison to model calculations (red solid line) allows determining the bond lengthening to 0.2 Å. Adapted from ref. [68].

between t_{2g} and e_g states) is larger than the pairing energy for the electrons, a low-spin (LS) complex is formed, as unpairing the electrons would be energetically unfavorable. The opposite is true for a smaller ligand field splitting, which leads to an unpairing of electrons and thus a high-spin complex (HS). Spin crossover can be induced by light, magnetic fields, and temperature or pressure jumps. Generally, spin-crossover complexes can potentially

serve as light-induced switches or molecular data storage devices. Spin-crossover dynamics in the prototypical Iron(II)-tris(bipyridine) ($[Fe(II)(bpy)_3]^{2+}$) complex have been studied extensively by ultrafast spectroscopy [122–124]. In particular the exact relaxation cascade that leads to the population of the HS state following photoexcitation from the LS state is a debated topic [125]. Femtosecond XANES studies at the Fe K-edge of $Fe(II)(bpy)_3]^{2+}$ resolved this controversy [68, 126]. The study is summarized in Fig. 4. Pump pulses centered at 266 nm excite the LS ground state to the singlet metal-to-ligand charge transfer state (^{1}MLCT, Fig. 4a), effectively reducing the metal center. In order to follow the subsequent dynamics, a previously established link was used: namely an increased XAS peak intensity at the Fe K edge is correlated with an increased Fe-N bond length, and different bond lengths have been established for the different complexes. The experiment by Bressler et al. [68] observed such an increase in the absorption edge after a relatively long delay of 50 ps (Fig. 4b), indicating that a long-lived HS complex corresponding to a $^5T_2$ quintuplet state is formed, which is the final product of a spin crossover of the photoexcited singlet MLCT state. Thus time-resolved measurements at the Fe K-edge (7126 eV) were used to indirectly follow the evolution of the bond length after photoexcitation. A step-like rise of the absorbance within 250-300 fs (Fig. 4c) indicated the ultrafast formation of the HS ($^5T_2$) complex. A comparison with a kinetic model confirmed the mechanism to be $^1A_1 + h\nu \rightarrow {}^1\text{MLCT} \rightarrow {}^3\text{MLCT} \rightarrow {}^5T$. While the photoexcitation to the singlet MLCT state is quasi instantaneous, the decay to the triplet state occurs within 20-30 fs and is thus below the experimental time sensitivity, but could possibly be observed with table-top x-ray high-harmonic sources.

V. ELECTRONIC AND STRUCTURAL DETERMINATION OF PHOTOCHEMICALLY ACTIVATED STRUCTURAL DYNAMICS

The femtosecond to picosecond dynamics and fundamental chemical reactivity in transition metal complexes is a heavily researched field due to the potential of the complexes for applications in solar energy conversion [127]. Spin crossover dynamics (previous section) and ligand loss upon photoexcitaion can create changes in the electronic and spin structure that can be characterized by suitable spectroscopic techniques. Furthermore structural changes will occur subsequently if the excited state is long lived. These also need to be measured and quantified. In this section, we describe two characteristic examples of such processes:

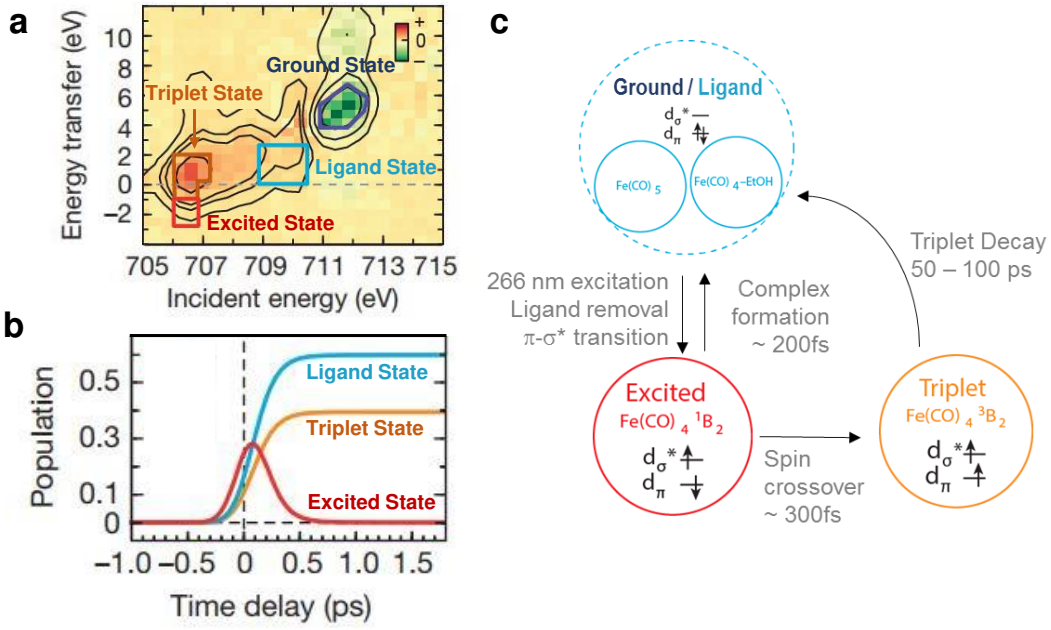

FIG. 5: **Time-resolved RIXS (FEL) of the ligand exchange dynamics in aqueous $Fe(CO)_5$:** (a) Differential excited state RIXS spectrum with highlighted areas of increased and decreased intensity that correspond to the ground, ligand, excited, and triplet state. (b) From the RIXS map in part (a) the excited state dynamics can be separated into the triplet and ligand state contributions. This would not have been possible in a x-ray absorption experiment due to the overlap of the triplet and excited state absorption energies. (c) Inferred excitation and relaxation pathway of the ligand exchange dynamics following photoexcitation. Adapted from ref. [86].

the ligand exchange dynamics in $Fe(CO)_5$ and structural deformation in a diplatinum complex following photoexcitation, which are investigated by resonant inelastic x-ray scattering (RIXS) and extended x-ray absorption fine structure spectroscopy (EXAFS), respectively. Both experiments were carried out in liquid environments.

In the first experiment (Fig. 5) a free flowing liquid jet of $Fe(CO)_5$ in ethanol was excited with 266 nm pump pulses [86], which remove a carbonyl ligand to produce $Fe(CO)_4$. RIXS spectra were recorded at the Fe $L_{2,3}$-edge around 710 eV, where core electrons from 2p orbitals are excited into an unoccupied valence state, and lower lying-electrons subsequently refill the core hole causing x-ray emission. The main intensity maximum in a static RIXS spectrum (not shown) is at 711.5 eV and corresponds to a $2p$ to $2\pi^*$ excitation with subse-

quent inelastic scattering to a lower lying state ($d_\pi^7 2\pi^{*1}$ configuration, 5.5 eV energy transfer). A difference RIXS spectrum is shown in Fig. 5a, where recorded spectra at negative delays were subtracted from the spectra at positive delays. The substantial changes across the spectrum following photoexcitation indicate the change in electronic and nuclear structure, which mainly occur due to changes in the $2p \rightarrow$LUMO resonance energy within the range 706.5 to 710 eV. Photoexcitation and ligand dissociation leave a hole in a d_π orbital, which is localized on the metal. The depletion of the ground state upon photoexcitation is apparent in the signal decrease in the violet region in Fig. 5(a,b), which is located right where the main RIXS signal of unexcited $Fe(CO)_5$ is located (not shown). In addition, photoexcitation introduces a new transition at lower energies (706.5 eV, excited state and triplet state) due to the created hole in the highest occupied molecular orbital (HOMO). The excited singlet state is generated briefly during photoexcitation with a lifetime of 200-300 fs (red region in Fig. 5(a,b)), either undergoing spin crossover (see last section) to form an excited triplet (300 fs lifetime, orange region in Fig. 5(a,b)), or it undergoes back-coordination with a CO or an EtOH ligand to form vibrationally hot re-ligated $Fe(CO)_5$ or $Fe(CO)_4EtOH$ (blue region in Fig. 5(a,b)). This back-coordination is close to the original RIXS peak (violet region) but slightly shifted as the newly formed $Fe(CO)_5$ is vibrationally hot, or $Fe(CO)_4EtOH$ is formed, and occurs with a time constant of about 200 fs. Importantly, this study RIXS could spectrally distinguish the singlet and triplet excited states (red and orange regions in Fig. 5(a,b)), which have similar x-ray absorption, but are characterized through different resonant emission features. The resulting mechanism is summarized in Fig. 5c. Upon photoexcitation from the ground state (blue field in Fig. 5c), a ligand is removed and an excited state is formed (red), which can either undergo re-ligation in about 200 fs, or undergo spin crossover in about 300 fs (orange), which subsequently decays back to the ground state on much longer time scales of about 50-100 ps.

Finally, the geometric structure of a complex will change upon photoexcitation to a long-lived excited state. Stroboscopic x-ray diffraction studies of the diplatinum complex $[Pt_2(P_2O_5H_2)_4]^4$ indicated a Pt-Pt bond shortening in the excited state [128]. Extended x-ray absorption fine structures can reveal structural changes, as variations in those are governed by scatterings events of the excited photoelectron with neighboring atoms. Therefore, subsequent EXAFS studies were carried out and revealed a shortening of the Pt-P and Pt-O separations in the excited state, but were insensitive to the Pt-Pt bond [129–131].

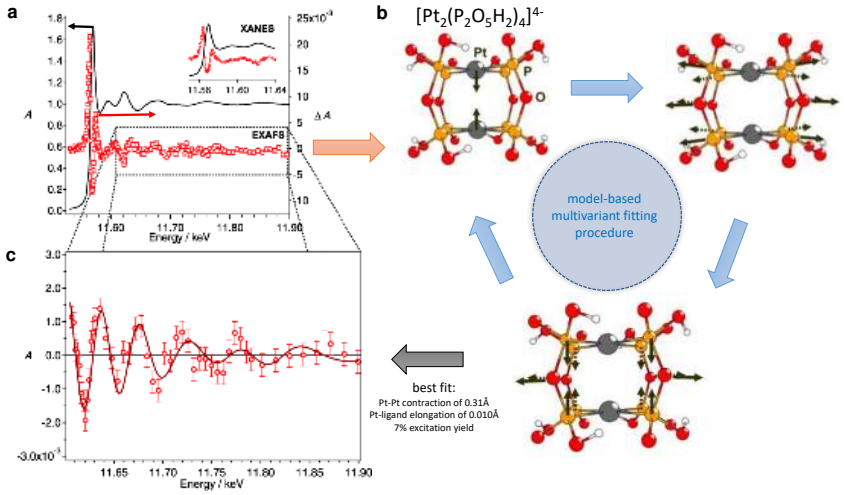

FIG. 6: **Time-resolved EXAFS measurement reveals structural dynamics of a photochemically active diplatinum molecule in solution** (a) Time-resolved EXAFS is recorded at the platinum L_3 edge (ground state absorbance in black) 150 ns following photoexcitation with 390 nm light (red data points). (b) Using a set of likely bond deformation scenarios EXAFS spectra are calculated and fitted to the experimental data (black line in (c). The excellent agreement with the feature-rich EXAFS spectra gives insight into bond deformation dynamics in complex aqueous molecules. Adapted from ref. [69].

Van der Veen et al. followed up on these experiments and excited a diplatinum complex $[Pt_2(P_2O_5H_2)_4]^{-2}$ at 370 nm into the first singlet excited state and probed its geometry through EXAFS by hard x-rays at the Pt L_3-edge (11.5-11.9 keV) [69]. Previous studies indicated a Pt-Pt bond shortening of 0.175-0.225 Åin the excited state by measuring the metal-metal stretch vibrational frequencies. EXAFS can provide a more direct picture of the global structural changes in the photoexcited complex. Transient EXAFS spectra are shown in Fig. 6, where the black spectrum shows the ground state absorption, and the red spectrum indicates the excited state. Oscillations versus energy can be predicted from an initial starting geometry of the diplatinum complex, which is iteratively varied to match the experimental spectrum. Following this procedure the model-based multivariant fitting procedure reveals the structure of the diplatinum complex, with a 0.31 A Pt-Pt bond length contraction and a 0.010 ÅPt-ligand elongation. The investigation of bond shortening of

dimetal complexes and structural changes by x-ray absorption and scattering techniques remains an active field of research [132–134]

VI. DISCUSSION AND OUTLOOK

In this perspective, we described the currently available x-ray techniques for time-resolved spectroscopy of chemical dynamic processes. Attosecond transient absorption and photofragmentation spectroscopy are able to elucidate the evolution of electronic coherences [65, 84], which occur on the sub-femtosecond to few-femtosecond time scale. After dephasing of the electronic coherences, more complex molecular processes can set in, and the newly developed capabilities of table-top carbon K-edge transient absorption spectroscopy [66, 67, 116] (and greater x-ray energy regimes) can be used to study dissociations and ring openings. Other preeminent dynamical processes like spin-crossover [68] and ligand-exchange dynamics [86] occur on similar time scales, and new techniques like RIXS can measure valence energy transfers, reminiscent of the valence energy level separations and core level transitions, simultaneously. Finally, the extended absorption fine structure studies in EXAFS give information on the evolving nuclear geometry [69].

While synchrotron sources for x-ray spectroscopy have been perfected over the last decades, the HHG based laboratory sources and FELs are still making tremendous improvements. Pulse durations at FELs have been continuously dropping over the last years and the bandwidths of single-spike pulses are supporting durations of about 200 attoseconds [27, 135], and are thus approaching the pulse durations achieved by HHG. High-harmonic generation based XUV and soft x-ray sources already provide the ultimate time resolution approaching the atomic unit of time (24 as) [21, 23]. Much development is now devoted to extending the accessible photon energies to spectroscopically access the very relevant carbon, oxygen and nitrogen K-edges, as well as the 3d transition metal L-edges, which will enable the study of ultrafast charge transfer and reaction dynamics of novel inorganic materials as well as photochemically active organic and organo-metallic complexes in gaseous, liquid and solid environments.

In particular, experiments on free-flowing thin liquid jets in vacuum have made tremendous progress in the last years [136]. The FEL and synchrotron studies on spin-crossover, and electronic and structural dynamics of photochemically activated species reported in this

perspectivee were done in liquid environments. Soft x-ray studies with high-harmonic sources have been hindered for a long time by the short penetration depths in liquids and solutes. The developments of free-flowing liquid jets [137–139] have allowed first high-harmonic based soft x-ray photoelectron studies on liquid samples [140], and many more studies, including transient absorption experiments, will follow in the future, which will shed light on larger and more complex molecules.

The field of x-ray spectroscopy is also undergoing a rapid technical development, in particular due to the developments of new free-electron lasers, as well as higher-flux, higher photon-energy HHG sources. New FEL sources are developed in the United States (LCLS II), the European Union (XFFEL in Germany), Switzerland (SwissFEL) and South Korea (PAL-FEL). They are now becoming available [97] and will deliver brighter and higher flux hard x-ray pulses. The femtosecond technology underlying high-harmonic generation is currently undergoing a rapid change. While Titanium:Sapphire lasers delivering 800 nm pulses have been the de-facto workhorses for generating high-harmonics in the XUV and soft x-ray range for the last twenty years, optical parametric chirped-pulse amplifiers (OPCPAs) are now challenging the pivotal role of Titanium:Sapphire systems. OPCPAs are capable of producing much higher average powers than Titanium:Sapphire systems, which can benefit the available pulse energies and repetition rates for driving HHG [141]. Additionally, OPCPAs have the advantage of wavelength tunability, which will enable the generation of photon energies up to 1 keV at high fluxes with HHG sources.

The high spatial coherence of the described x-ray sources have opened up new paths for imaging nanoscale targets and probing their dynamics with femtosecond time resolution. Transient states of xenon nanoparticles were imaged by x-ray scattering by FEL lasers [142], and single helium nanodroplets were imaged with a high-harmonic source [143]. These experiments pave the way towards nanoscale imaging experiments with few-femtosecond to attosecond time resolution. Such scattering techniques will be crucial for studying the initial steps of heterogeneous catalytic reaction cycles [144] of molecules on nano-structured surfaces.

The recent development of table-top high harmonic sources with circular polarization [34, 145] enable soft x-ray experiments on magnetic materials [146] and chiral molecules [147]. Such sources can even be combined with the previously mentioned scattering techniques on nano-structured samples [148], which has been used to image magnetic domains, and will

enable the investigation the demagnetization dynamics of structured magnetic materials.

A major driving force behind the construction of FELs is imaging biomolecular systems such as proteins by femtosecond X-ray nanocrystallography [149]. However, the high intensities required for such imaging experiments induce multiple ionization events and subsequent fragmentation of the proteins [150], which requires the use of very short pulses of a few femtosecond duration, as well as a thorough understanding of the ionization dynamics upon x-ray exposure. Pioneering experiments have investigated the formation of highly charged neon ions after x-ray exposure [151]. Future experiments could use core-ionization to trigger ultrafast subfemtosecond charge migration [152], which could be probed with element specificity by broadband attosecond absorption measurements.

While this perspective reviews the achievements of pump-probe techniques, further developments of high-brilliance sources and attosecond multi-pulse experiments will enable novel x-ray multidimensional spectroscopy. Theoretical research has already explored numerous opportunities [153], and first experimental steps in this direction have successfully implemented four-wave mixing experiments (XUV + 2 near infrared photons) in nobles gases [154–156]. First experiments have already been successful in demonstrating non-linear x-ray interactions in solids: Hard X-ray and optical sum-frequency [157] generation as well as soft x-ray surface second-harmonic generation [158] have been demonstrated at FELs. Hard x-ray interactions induce second-harmonic and sum-frequency generation even in centrosymmetric bulk materials due to optically induced charges fields arising in the exposed sample. On the other hand, soft x-ray surface second-harmonic generation can be a true interface probe due to the longer wavelength, much like optical surface second-harmonic generation spectroscopy and will provide a new route to studying ultrafast interface dynamics. In general, multidimensional x-ray techniques will have the potential to elegantly separate core-level shifts from valence shell dynamics and to correlate the induced chemical dynamics to the local environment of single atoms in molecules. As such, multidimensional x-ray techniques can bring another revolution to the studies of chemical dynamics and chemical structure, much like multidimensional NMR, infrared and visible techniques have provided fundamental new insight into chemical science.

Acknowledgments

We acknowledge funding from the Air Force Office of Scientific Research (AFOSR) (grants no. FA9550-15-1-0037 and FA9550-14-1-0154), the Army Research Office (ARO) (WN911NF-14-1-0383), the Office of Assistant Secretary of Defense for Research and Engineering through a National Security Science and Engineering Faculty Fellowship (NSSEFF), the W. M. Keck Foundation, the Defense Advanced Research Projects Agency PULSE program through grant W31P4Q-13-1-0017, and the National Science Foundation (NSF) through grants CHE-1361226 and CHE-1660417, and through a Foundation Major Research Instrumentation (NSF MRI) grant #1624322. Further funding was provided by the U.S. Department of Energy, Office of Science, Office of Basic Energy Sciences, Atomic, Molecular and Optical Sciences Program, and Physical Chemistry of Inorganic Nanostructures Program under Contract No. DE-AC02-05-CH11231. P. M. K. acknowledges support from the Swiss National Science Foundation (grants no. P2EZP2_165252 and P300P2_174293). M. Z. acknowledges support from the Humboldt Foundation. S.K.C. is supported by the Department of Energy, Office of Energy Efficiency and Renewable Energy (EERE) Postdoctoral Research Award under the EERE Solar Energy Technologies Office.

[1] M. Eigen, Discuss. Faraday Soc. **17**, 194 (1954).

[2] G. Porter, Discuss. Faraday Soc. **9**, 60 (1950).

[3] Nobelprize.org, http://www.nobelprize.org/nobel_prizes/chemistry/laureates/1967 (retrieved on November 10, 2017).

[4] M. Dantus, M. J. Rosker, and A. H. Zewail, The Journal of Chemical Physics **87**, 2395 (1987).

[5] M. J. Rosker, M. Dantus, and A. H. Zewail, Science **241**, 1200 (1988).

[6] T. S. Rose, M. J. Rosker, and A. H. Zewail, The Journal of Chemical Physics **91**, 7415 (1989).

[7] A. Mokhtari, P. Cong, J. Herek, and A. Zewail, Nature **348**, 225 (1990).

[8] M. Dantus, R. M. Bowman, M. Gruebele, and A. H. Zewail, The Journal of Chemical Physics **91**, 7437 (1989).

[9] Nobelprize.org, http://www.nobelprize.org/nobel_prizes/chemistry/laureates/1999 (retrieved on November 10, 2017).

[10] M. Minitti et al., Physical review letters **114**, 255501 (2015).

[11] H. Ihee et al., Science **291**, 458 (2001).

[12] J. M. Glownia et al., Phys. Rev. Lett. **117**, 153003 (2016).

[13] Z.-H. Loh and S. R. Leone, The Journal of Physical Chemistry Letters **4**, 292 (2013), PMID: 26283437.

[14] E. R. Hosler and S. R. Leone, Phys. Rev. A **88**, 023420 (2013).

[15] A. D. Dutoi and S. R. Leone, Chemical Physics **482**, 249 (2017).

[16] Z. Wei et al., Nature Communications **8**, 735 (2017).

[17] K. Ramasesha, S. R. Leone, and D. M. Neumark, Annual Review of Physical Chemistry **67**, 41 (2016).

[18] M. Hentschel et al., Nature **414**, 509 (2001).

[19] E. Goulielmakis et al., Science **320**, 1614 (2008).

[20] K. Zhao et al., Optics letters **37**, 3891 (2012).

[21] J. Li et al., Nature Communications **8**, 186 (2017).

[22] S. L. Cousin et al., Physical Review X **7**, 041030 (2017).

[23] T. Gaumnitz et al., Optics Express **25**, 27506 (2017).

[24] R. Mitzner et al., Physical Review A **80**, 025402 (2009).

[25] R. Moshammer et al., Optics express **19**, 21698 (2011).

[26] W. Helml et al., Nature photonics **8**, 950 (2014).

[27] S. Huang et al., Physical Review Letters **119**, 154801 (2017).

[28] R. Schoenlein et al., Science **287**, 2237 (2000).

[29] L. X. Chen, Annual Review of Physical Chemistry **56**, 221 (2005), PMID: 15796701.

[30] L. Chen, X. Zhang, and M. Shelby, Chemical Science **5**, 4136 (2014).

[31] L.-O. Chan et al., Physical Review Letters **103**, 257402 (2009).

[32] M. Schultze et al., Science **346**, 1348 (2014).

[33] C.-M. Jiang et al., J. Phys. Chem. C **118**, 22774 (2014).

[34] O. Kfir et al., Nature Photonics **9**, 99 (2015).

[35] I. Gierz et al., Physical review letters **115**, 086803 (2015).

[36] M. Lucchini et al., Science **353**, 916 (2016).

[37] M. Zürch et al., Nature Comm. **8**, 15734 (2017).

[38] M. F. Jager et al., Proceedings of the National Academy of Sciences **114**, 9558 (2017).

[39] L. M. Carneiro et al., Nature Materials **16**, 819 (2017).

[40] A. Moulet et al., Science **357**, 1134 (2017).

[41] A. L. Cavalieri et al., Nature **449**, 1029 (2007).

[42] M. Schultze et al., Science **328**, 1658 (2010).

[43] Z. Tao et al., Science **353**, 62 (2016).

[44] H. Wang et al., Phys. Rev. Lett. **105**, 143002 (2010).

[45] M. Lein, Phys. Rev. Lett. **94**, 053004 (2005).

[46] S. Baker et al., Science **312**, 424 (2006).

[47] O. Smirnova et al., Nature **460**, 972 (2009).

[48] S. Haessler et al., Nat. Phys. **6**, 200 (2010).

[49] P. M. Kraus et al., Science **350**, 790 (2015).

[50] J. Itatani et al., Nature **432**, 867 (2004).

[51] C. Vozzi et al., Nat Phys **7**, 822 (2011).

[52] H. J. Wörner, H. Niikura, J. B. Bertrand, P. B. Corkum, and D. M. Villeneuve, Phys. Rev. Lett. **102**, 103901 (2009).

[53] A. D. Shiner et al., Nature Physics **7**, 464 (2011).

[54] P. M. Kraus, D. Baykusheva, and H. J. Wörner, Phys. Rev. Lett. **113**, 023001 (2014).

[55] P. M. Kraus et al., Nat. Commun. **6**, 7039 (2015).

[56] H. J. Wörner, J. B. Bertrand, D. V. Kartashov, P. B. Corkum, and D. M. Villeneuve, Nature **466**, 604 (2010).

[57] A. Tehlar and H. J. Wörner, Molecular Physics **111**, 2057 (2013).

[58] H. J. Wörner et al., Science **334**, 208 (2011).

[59] P. M. Kraus et al., Phys. Rev. A **85**, 043409 (2012).

[60] P. M. Kraus and H. J. Wörner, Chemical Physics **414**, 32 (2013).

[61] S. Ghimire et al., Nature physics **7**, 138 (2011).

[62] G. Vampa et al., Physical review letters **115**, 193603 (2015).

[63] R. Silva, I. V. Blinov, A. N. Rubtsov, O. Smirnova, and M. Ivanov, arXiv preprint arXiv:1704.08471 (2017).

[64] A. R. Beck, D. M. Neumark, and S. R. Leone, Chemical Physics Letters **624**, 119 (2015).

[65] E. Goulielmakis et al., Nature **466**, 739 (2010).

[66] A. R. Attar et al., Science **356**, 54 (2017).

[67] Y. Pertot et al., Science **355**, 264 (2017).

[68] C. Bressler et al., Science **323**, 489 (2009).

[69] R. M. vanderVeen et al., Angewandte Chemie International Edition **48**, 2711 (2009).

[70] U. Bergmann and P. Glatzel, Photosynthesis research **102**, 255 (2009).

[71] M. Haumann et al., Science **310**, 1019 (2005).

[72] M. E. Vaida and S. R. Leone, The Journal of Physical Chemistry C **120**, 2769 (2016).

[73] B. M. Marsh, M. E. Vaida, S. K. Cushing, B. R. Lamoureux, and S. R. Leone, The Journal of Physical Chemistry C **121**, 21904 (2017).

[74] K. R. Siefermann et al., The journal of physical chemistry letters **5**, 2753 (2014).

[75] T. Arion et al., Applied Physics Letters **106**, 121602 (2015).

[76] S. Neppl and O. Gessner, Journal of Electron Spectroscopy and Related Phenomena **200**, 64 (2015).

[77] A. Gray et al., Nature Materials **10**, 759 (2011).

[78] S. Mathias et al., Review of Scientific Instruments **78**, 083105 (2007).

[79] S. Eich et al., Journal of Electron Spectroscopy and Related Phenomena **195**, 231 (2014).

[80] T. Rohwer et al., Nature **471**, 490 (2011).

[81] S. Hellmann et al., Nature Communications **3**, 1069 (2012).

[82] H. Wang et al., Nature communications **6**, 7459 (2015).

[83] L. Belshaw et al., The Journal of Physical Chemistry Letters **3**, 3751 (2012).

[84] F. Calegari et al., Science **346**, 336 (2014).

[85] G. Sansone et al., Nature **465**, 763 (2010).

[86] P. Wernet et al., Nature **520**, 78 (2015).

[87] T. Popmintchev et al., Science **336**, 1287 (2012).

[88] J. Biegert and co workers, private communication (2017).

[89] E. Takahashi, Y. Nabekawa, T. Otsuka, M. Obara, and K. Midorikawa, Physical Review A **66**, 021802 (2002).

[90] G. Sansone, L. Poletto, and M. Nisoli, Nature Photonics **5**, 655 (2011).

[91] E. Goulielmakis et al., Science **317**, 769 (2007).

[92] H. Timmers et al., Optica **3**, 707 (2016).

[93] S. Hädrich et al., Journal of Physics B: Atomic, Molecular and Optical Physics **49**, 172002 (2016).

[94] A. Cingöz et al., Nature **482**, 68 (2012).

[95] D. T. Reid et al., Journal of Optics **18**, 093006 (2016).

[96] https://www.xfel.eu/facility/comparison/index_eng.html, retrieved on Feb 5, 2018.

[97] L. Young et al., Journal of Physics B: Atomic, Molecular and Optical Physics **51**, 032003 (2018).

[98] C. Bressler and M. Chergui, Chemical reviews **104**, 1781 (2004).

[99] R. J. Jones, K. D. Moll, M. J. Thorpe, and J. Ye, Physical Review Letters **94**, 193201 (2005).

[100] I. Pupeza et al., Nature Photonics **7**, 608 (2013).

[101] D. Charalambidis et al., Eli-alps, the attosecond facility of the extreme light infrastructure, in *The European Conference on Lasers and Electro-Optics*, page CG_4_1, Optical Society of America, 2013.

[102] S. Kühn et al., Journal of Physics B: Atomic, Molecular and Optical Physics **50**, 132002 (2017).

[103] C. Arnold, O. Vendrell, and R. Santra, Physical Review A **95**, 033425 (2017).

[104] G. S. Engel et al., Nature **446**, 782 (2007).

[105] G. D. Scholes et al., Nature **543**, 647 (2017).

[106] P. W. Shor, Physical review A **52**, R2493 (1995).

[107] J. I. Cirac and P. Zoller, Physical review letters **74**, 4091 (1995).

[108] D. Loss and D. P. DiVincenzo, Physical Review A **57**, 120 (1998).

[109] L. Cederbaum and J. Zobeley, Chemical Physics Letters **307**, 205 (1999).

[110] J. Breidbach and L. S. Cederbaum, J. Chem. Phys. **118**, 3983 (2003).

[111] F. Remacle and R. D. Levine, PNAS **103**, 6793 (2006).

[112] J. Breidbach and L. S. Cederbaum, Phys. Rev. Lett. **94**, 033901 (2005).

[113] G. Sansone, T. Pfeifer, K. Simeonidis, and A. I. Kuleff, ChemPhysChem **13**, 661 (2012).

[114] A. I. Kuleff, S. Lünnemann, and L. S. Cederbaum, Chemical Physics **414**, 100 (2013).

[115] A. I. Kuleff and L. S. Cederbaum, Journal of Physics B: Atomic, Molecular and Optical Physics **47**, 124002 (2014).

[116] A. Bhattacherjee, C. D. Pemmaraju, K. Schnorr, A. R. Attar, and S. R. Leone, Journal of the American Chemical Society **139**, 16576 (2017).

[117] F. Lackner et al., The Journal of chemical physics **145**, 234313 (2016).

[118] A. S. Chatterley, F. Lackner, D. M. Neumark, S. R. Leone, and O. Gessner, Physical Chemistry Chemical Physics **18**, 14644 (2016).

[119] A. S. Chatterley et al., The Journal of Physical Chemistry A **120**, 9509 (2016).

[120] A. R. Attar, A. Bhattacherjee, and S. R. Leone, The journal of physical chemistry letters **6**, 5072 (2015).

[121] A. Cavalleri et al., Physical Review Letters **95**, 067405 (2005).

[122] J. K. McCusker et al., Journal of the American Chemical Society **115**, 298 (1993).

[123] J. E. Monat and J. K. McCusker, Journal of the American Chemical Society **122**, 4092 (2000).

[124] W. Gawelda et al., Journal of the American Chemical Society **129**, 8199 (2007).

[125] C. Brady, J. J. McGarvey, J. K. McCusker, H. Toftlund, and D. N. Hendrickson, *Time-Resolved Relaxation Studies of Spin Crossover Systems in Solution*, pages 1–22, Springer Berlin Heidelberg, Berlin, Heidelberg, 2004.

[126] M. Khalil et al., The Journal of Physical Chemistry A **110**, 38 (2006).

[127] B. E. Van Kuiken et al., The journal of physical chemistry letters **3**, 1695 (2012).

[128] C. D. Kim, S. Pillet, G. Wu, W. K. Fullagar, and P. Coppens, Acta Crystallographica Section

A: Foundations of Crystallography **58**, 133 (2002).

[129] N. Yasuda, M. Kanazawa, H. Uekusa, and Y. Ohashi, Chemistry letters **31**, 1132 (2002).

[130] Y. Ozawa et al., Chemistry letters **32**, 62 (2002).

[131] N. Yasuda, H. Uekusa, and Y. Ohashi, Bulletin of the Chemical Society of Japan **77**, 933 (2004).

[132] I. V. Novozhilova, A. V. Volkov, and P. Coppens, Journal of the American Chemical Society **125**, 1079 (2003).

[133] J. V. Lockard et al., The Journal of Physical Chemistry A **114**, 12780 (2010).

[134] K. Haldrup et al., Inorganic chemistry **50**, 9329 (2011).

[135] A. Marinellia et al., Appl. Phys. Lett. **111**, 151101 (2017).

[136] M. H. Elkins, H. L. Williams, A. T. Shreve, and D. M. Neumark, Science **342**, 1496 (2013).

[137] M. Faubel, S. Schlemmer, and J. Toennies, Zeitschrift für Physik D Atoms, Molecules and Clusters **10**, 269 (1988).

[138] M. Faubel, B. Steiner, and J. P. Toennies, The Journal of Chemical Physics **106**, 9013 (1997).

[139] M. Faubel, K. R. Siefermann, Y. Liu, and B. Abel, Acc. Chem. Res. **45**, 120 (2012).

[140] K. R. Siefermann and B. Abel, Angew. Chem. Int. Ed. **50**, 5264 (2011).

[141] H. Fattahi et al., Optica **1**, 45 (2014).

[142] C. Bostedt et al., Phys. Rev. Lett. **108**, 093401 (2012).

[143] D. Rupp et al., Nature communications **8**, 493 (2017).

[144] S. Bordiga, E. Groppo, G. Agostini, J. A. van Bokhoven, and C. Lamberti, Chemical reviews **113**, 1736 (2013).

[145] A. Fleischer, O. Kfir, T. Diskin, P. Sidorenko, and O. Cohen, Nature Photonics **8**, 543 (2014).

[146] T. Fan et al., Proceedings of the National Academy of Sciences **112**, 14206 (2015).

[147] S. Beaulieu et al., Science **358**, 1288 (2017).

[148] O. Kfir et al., Science advances **3**, eaao4641 (2017).

[149] H. N. Chapman et al., Nature **470**, 73 (2011).

[150] R. Neutze, R. Wouts, D. van der Spoel, E. Weckert, and J. Hajdu, Nature **406**, 752 (2000).

[151] L. Young et al., Nature **466**, 56 (2010).

[152] A. I. Kuleff, N. V. Kryzhevoi, M. Pernpointner, and L. S. Cederbaum, Physical review letters **117**, 093002 (2016).

[153] S. Mukamel, D. Healion, Y. Zhang, and J. D. Biggs, Annual Review of Physical Chemistry **64**, 101 (2013).

[154] W. Cao, E. R. Warrick, A. Fidler, S. R. Leone, and D. M. Neumark, Phys. Rev. A **94**, 021802 (2016).

[155] W. Cao, E. R. Warrick, A. Fidler, D. M. Neumark, and S. R. Leone, Phys. Rev. A **94**, 053846 (2016).

[156] T. Ding et al., Opt. Lett. **41**, 709 (2016).

[157] T. Glover et al., Nature **488**, 603 (2012).

[158] R. K. Lam et al., Phys. Rev. Lett. **120**, 023901 (2018).